RSC Advances

PAPER

View Article Online
View Journal | View Issue



Cite this: *RSC Adv.*, 2023, **13**, 27957

# Spectral properties of $B_{40}$ enhanced by small molecule adsorption†

Jia Wang,[a] Yunkai Zhang,[a] Meiqi Wang,[a] Ming-Xing Song,[a] Bo Wang*[b] and Zhengkun Qin*[a]

The luminescence characteristics of small molecule excited $B_{40}$ have not been studied yet, and it may have a potential application value in quantum dot luminescence. Herein, the adsorption and fluorescence emission spectra of small molecules (pyridine, pyrazine and benzene) adsorbed on $B_{40}$ are studied using first-principles. The results show that the absorption of pyridine and pyrazine on $B_{40}$ can form stable chemisorption structures pyridine-$B_{40}$ and pyrazine-$B_{40}$, while benzene adsorption can form physisorption structure benzene-$B_{40}$. Moreover, the adsorbed pyridine can enhance the intensity of emission spectra of $B_{40}$. And the pyrazine adsorbed can obviously enhance the intensity of absorption and emission spectra of $B_{40}$ and cause the spectra to redshift to the visible light range. And the adsorption of benzene has almost no enhancement effect on absorption and emission spectra of $B_{40}$. In addition, the influence of different computational basis sets on spectra characteristics has also been discussed and the results show that the main peaks of absorption and emission spectra calculated by the diffuse function augmented basis sets are redshifted relatively. This finding provides a strategy for quantum dot luminescence and a theoretical reference for experimental research.

Received 11th July 2023
Accepted 14th September 2023

DOI: 10.1039/d3ra04631a

rsc.li/rsc-advances



## Introduction

All-boron fullerenes $B_{40}$ were discovered by a combination of experiment and theory in 2014.[1] Subsequent theoretical studies revealed that $B_{40}$ is a superatom.[2] And the chain-like assembly with $B_{40}$ superatom has also been studied, which show that the assembly can decrease band gap and achieve transformation from insulator to a semiconductor.[3] Moreover, due to the electron deficiency of boron fullerenes,[4,5] adsorbed or doped additional atoms or small molecules on them may form more stable structures. The adsorption behaviors of $B_{40}$ nanocage towards aniline is reported, and doping $B_{40}$ with Mn and Fe atoms can be an efficient approach for the removal of aniline.[6] And atom adsorbed or doped $B_{40}$ can improve hydrogen storage capacity of $B_{40}$.[7–10] Therefore, adsorbed or doped atoms or small molecules on the surface of $B_{40}$ fullerene may also enhance its other properties, such as fluorescence spectra.

Previous studies have found that superatoms have unique spectral properties, such as $C_{60}$,[11] $Na_{40}$,[12] $Al_{13}^-$ [13] and $Au_{20}$,[14] *etc.* The spectra of $B_{40}$ fullerene is also been investigated and distinguished the hollow cage structure from other quasi-planar structures.[15] Moreover, the spectral properties of metal-loborospherenes $MB_{40}^{0/-}$ (M = Cu, Ag, Au) are also studied, and the results suggest that doped metal atoms in borospherene $B_{40}$ can change the spectral features since the extra metal atoms can modify the electronic structure of $B_{40}$.[16] Nonlinear optical (NLO) features of metals decorated $B_{40}$ fullerene are studied and show remarkable electro-optical response.[17,18] Can the small molecules with strong electronegativity, such as the benzene, enhance or change the spectral characteristics when they adsorbed on $B_{40}$?

In this work, the adsorption of small molecules (pyridine, pyrazine and benzene) on all-boron fullerene $B_{40}$ is investigated by density functional theory (DFT).[19] The results show that the adsorbed small molecules can strengthen the absorption and emission spectra of $B_{40}$. The absorption and emission spectra of pyrazine-$B_{40}$ are in the visible light range. The purpose of this work is to gain the influence of small molecule on the spectra of $B_{40}$, and how these effects could be used to design quantum dot luminescence.

## Models and computational methods

In this work, the model is built by adsorbing small molecules (pyridine, pyrazine and benzene) on the $B_{40}$ cage. Due to $B_{40}$ fullerene has two heptagons and four hexagons,[1,2,20] the pyridine, pyrazine and benzene are adsorbed at hexagon, heptagon and B atom sites of $B_{40}$ fullerene to form studied structures.

[a]*College of Information Technology, Jilin Engineering Research Center of Optoelectronic Materials and Devices, Jilin Normal University, Siping, 136000, China. E-mail: qzkjlnu@163.com*

[b]*School of Science, Northeast Electric Power University, Jilin, 131200, China. E-mail: bowang@neepu.edu.cn*

† Electronic supplementary information (ESI) available: The adsorption energy analysis, the calculation details about structural optimization and the analysis of electronic density difference. See DOI: https://doi.org/10.1039/d3ra04631a

After theoretical simulation and structural optimization, the six stable geometric structures are obtained, as presented in Fig. 1. Fig. 1a shows that the N atom of pyridine is bonded with the B atom of $B_{40}$ (denoted as pyridine-$B_{40}$), and Fig. 1b shows that pyridine is adsorbed at the hexagon of $B_{40}$ (pyridine-$B_{40}$-6), the former has the lowest energy. Fig. 1c and d show that the N atom of pyrazine is bonded with B atom of $B_{40}$ and the pyrazine is adsorbed at heptagon of $B_{40}$, denoted as pyrazine-$B_{40}$ and pyrazine-$B_{40}$-7, respectively, and the former have the lowest energy. It can be seen that the chemisorption structures are more stable than the physisorption structures. Besides, Fig. 1e and f show that the benzene are respectively adsorbed at hexagon and heptagon of $B_{40}$ (denoted as benzene-$B_{40}$-6 and benzene-$B_{40}$-7), and they are physisorption structures. Compared with benzene-$B_{40}$-7, the benzene-$B_{40}$-6 has lower energy. In addition, we further verified it by adsorption energy decomposition, and the results show that the benzene-$B_{40}$-6 is more stable than benzene-$B_{40}$-7 structure. The detailed adsorption energy analysis is placed in the first part in the ESI.† The relative energies between each isomer and the lowest energy structure are listed in brackets. In the following, we mainly analysed the three structures with the lowest energy, that is, pyridine-$B_{40}$, pyrazine-$B_{40}$ and benzene-$B_{40}$-6.

The empirical dispersion-corrected density functional theory (DFT-D3)[21] is used to fully optimize the geometric structures by hybrid functionals PBE0[22] with 6-31G* basis sets.[23] All the optimized structures are confirmed to be local minima. The calculation details are placed in the second part in the ESI.† Simultaneously, based on the geometric structures, TD-DFT method[19,24] is used to calculate the electronic transition, absorption and emission spectral properties. And we chose the range-separated hybrid functionals CAM-B3LYP[25,26] to calculate the absorption and emission spectra with 6-31G*, 6-31+G* and 6-311+G* basis sets.[27] For accurate calculation, we selected 30 and 10 electronic states in the adsorption and emission spectra for calculation. In addition, all the computations are carried out using the Gaussian16 software package.[28]

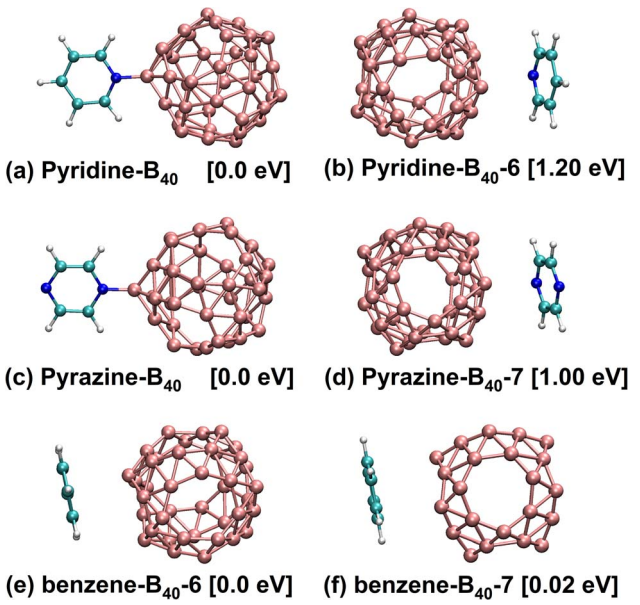


Fig. 1 Structural diagram of pyridine-$B_{40}$, pyrazine-$B_{40}$ and benzene-$B_{40}$ at PBE0/6-31G* level. (a) and (b) The N atom of pyridine is bonded with the B atom of $B_{40}$ and pyridine is adsorbed at the hexagon of $B_{40}$. (c) and (d) The N atom of pyrazine is bonded with B atom of $B_{40}$ and the pyrazine is adsorbed at heptagon of $B_{40}$ respectively. (e) and (f) Benzene adsorbed at hexagon and heptagon of $B_{40}$, respectively. The values in brackets are the relative energies between each isomer and the lowest energy structures. Pink, cyan and blue in structures represent B, C and N atoms, respectively.

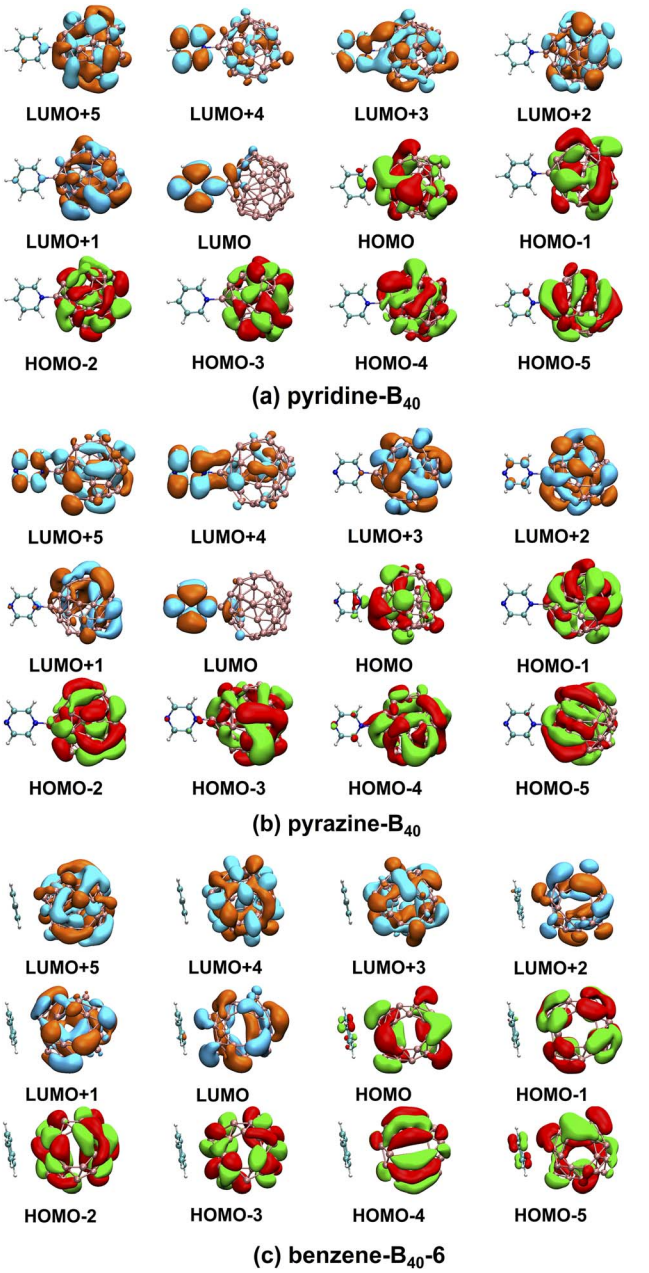


Fig. 2 The frontier MOs for (a) pyridine-$B_{40}$, (b) pyrazine-$B_{40}$, (c) benzene-$B_{40}$-6 at PBE0/6-31G* level. The MOs indicated by green and red are occupied MOs, while those indicated by orange and blue are unoccupied MOs. The isosurface value is 0.02 a.u.

## Results and discussion

Our calculations show that the ground states of pyridine-, pyrazine-, and benzene-$B_{40}$ are non-spin-polarized singlet, and the diagram of frontier molecular orbitals (MOs) is shown in Fig. 2. For pyridine-$B_{40}$ structure (Fig. 2a), the lowest unoccupied molecular orbital plus 5 (LUMO+5), LUMO+2, LUMO+1, the highest occupied molecular orbital (HOMO), HOMO−1, HOMO−2, HOMO−3, HOMO−4 and HOMO−5 mainly occupies on $B_{40}$, and the LUMO mainly occupy on pyridine. Moreover, the LUMO+4 and LUMO+3 are delocalization on $B_{40}$ and pyridine. Similar to pyridine-$B_{40}$, the LUMO+3, LUMO+2, LUMO+1, HOMO, HOMO−1, HOMO−2, HOMO−3, HOMO−4 and HOMO−5 of pyrazine-$B_{40}$ mainly occupy on $B_{40}$, the LUMO+4 and LUMO mainly occupy on pyridine (shown in Fig. 2b). And the LUMO+5 are delocalization on the whole structure. Different from pyridine-$B_{40}$ and pyrazine-$B_{40}$, the frontier MOs of benzene-$B_{40}$-6 mainly occupy on $B_{40}$ (as see Fig. 2c). Thus, the electrons in the pyridine-$B_{40}$ and pyrazine-$B_{40}$ structures transition from $B_{40}$ to small molecules, while for the benzene-$B_{40}$-6 structure, the electrons transition from $B_{40}$ to $B_{40}$.

To analyze the spectral characteristics of small molecule excitation $B_{40}$, the UV-vis absorption and emission spectra of the singlet excited states are shown in Fig. 3. The black, red, blue and green lines in the figure represent the absorption and emission spectra of the $B_{40}$, pyridine-$B_{40}$, pyrazine-$B_{40}$, and benzene-$B_{40}$-6 structures. Fig. 3a shows that the absorption spectrum of $B_{40}$ is localized around 350 nm, in the ultraviolet (UV) light range. And small molecules adsorbed not only enhance the intensity of the adsorption spectrum of $B_{40}$, but also redshift the spectrum from UV to visible light range. As see the red curve in the Fig. 3a, although the intensity of the absorption spectrum of pyridine-$B_{40}$ is not stronger than that of $B_{40}$ (black curve), the main absorption peak is relatively redshifted. Furthermore, the data of four typical absorption peaks for pyridine-$B_{40}$ are listed in Table 1. The first strong absorption peak is localized near 356 nm and the lowest single excited transition $S_0 \rightarrow S_1$ ($S_0$ and $S_1$ represent the ground state and first singlet excited state) mainly originates from the transition from the HOMO, HOMO−5 and HOMO−6 to the LUMO, LUMO+3 and LUMO+4, that is, the $S_0 \rightarrow S_1$ originates from the transition from $B_{40}$ to $B_{40}$ and pyridine. The second absorption peak near 358 nm arises from the HOMO−5 to LUMO and LUMO+3 transitions, similar discussions way have also been reflected in other works.[29] The other two typical absorption peaks are relatively weaker and localized near 429 nm and 445 nm, originating from the transition from HOMO, HOMO−1, HOMO−2, HOMO−3 and HOMO−4 to LUMO, LUMO+1, LUMO+2 and LUMO+3. Thus, the main adsorption peaks of pyridine-$B_{40}$ originate from the transition from $B_{40}$ to $B_{40}$ and pyridine.

Further, the UV-vis absorption spectrum of $S_0 \rightarrow S_1$ for pyrazine-$B_{40}$ is shown in the blue curve in Fig. 3a, and the data of four typical absorption peaks are also listed in Table 1. The first strong absorption peak near 437 nm originates from the HOMO−1, HOMO−3 and HOMO−4 to LUMO transition. The

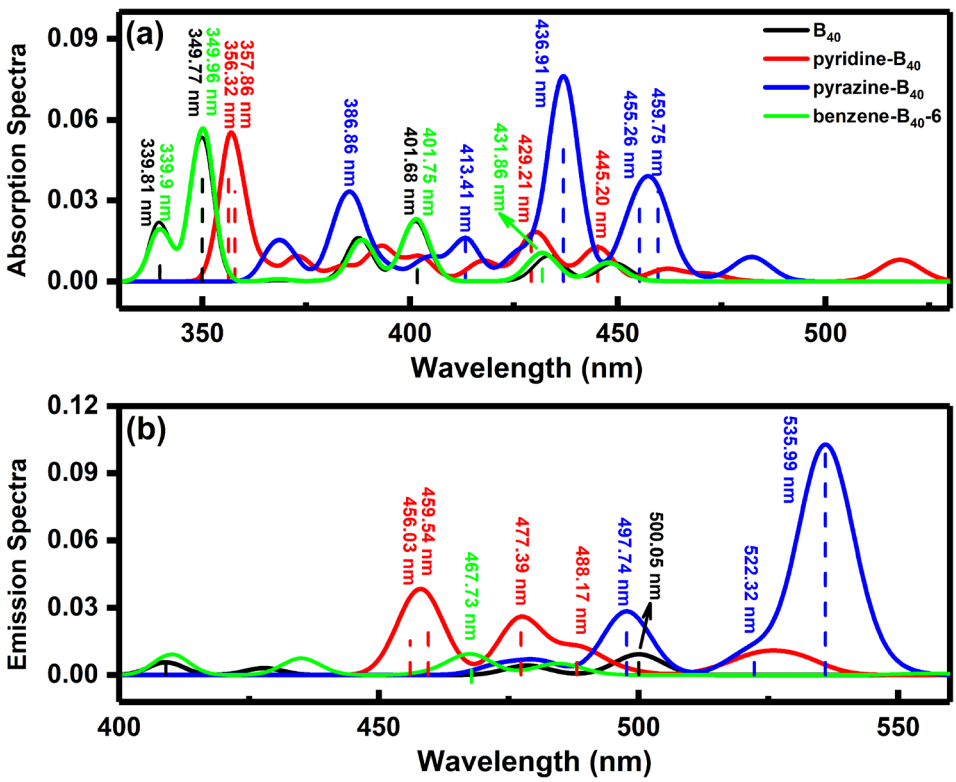


Fig. 3 (a) The absorption spectra of $B_{40}$, pyridine-$B_{40}$, pyrazine-$B_{40}$, and benzene-$B_{40}$-6 structures at CAM-B3LYP/6-31G* level; (b) The emission spectra of $B_{40}$, pyridine-$B_{40}$, pyrazine-$B_{40}$, and benzene-$B_{40}$-6 at CAM-B3LYP/6-31G* level.

Table 1 The absorption properties of the $B_{40}$, pyridine-$B_{40}$, pyrazine-$B_{40}$ and benzene-$B_{40}$-6 ($E$ is the excitation energy (eV), $\lambda$ is the absorption wavelength (nm), $f$ is the oscillator strength)

| Structures | States | $E/\lambda$ | $f$ | Main configuration (transitions) | Assignment |
|---|---|---|---|---|---|
| $B_{40}$ | $S_{28}$ | 3.65/339.81 | 0.0163 | HOMO−7 → LUMO+1 (34%)<br>HOMO−7 → LUMO+2 (48%) | $B_{40}$ → $B_{40}$ |
| | $S_{26}$ | 3.54/349.77 | 0.0795 | HOMO−6 → LUMO+2 (44%)<br>HOMO−5 → LUMO+1 (44%) | $B_{40}$ → $B_{40}$ |
| | $S_{10}$ | 3.09/401.68 | 0.0194 | HOMO−3 → LUMO+2 (21%)<br>HOMO−2 → LUMO+1 (21%)<br>HOMO → LUMO+3 (59%) | $B_{40}$ → $B_{40}$ |
| | $S_4$ | 2.86/433.54 | 0.0121 | HOMO−1 → LUMO (66%) | $B_{40}$ → $B_{40}$ |
| Pyridine-$B_{40}$ | $S_{30}$ | 3.48/356.32 | 0.0485 | HOMO−6 → LUMO+3 (25%)<br>HOMO−5 → LUMO (23%)<br>HOMO → LUMO+4 (29%) | $B_{40}$ → $B_{40}$ and pyridine |
| | $S_{29}$ | 3.46/357.86 | 0.0253 | HOMO−5 → LUMO (21%)<br>HOMO−5 → LUMO+3 (22%) | $B_{40}$ → $B_{40}$ and pyridine |
| | $S_9$ | 2.89/429.21 | 0.0153 | HOMO−4 → LUMO (27%)<br>HOMO−4 → LUMO+1 (31%)<br>HOMO−3 → LUMO+2 (22%)<br>HOMO → LUMO + 2 (26%)<br>HOMO → LUMO + 3 (24%) | $B_{40}$ → $B_{40}$ and pyridine |
| | $S_5$ | 2.78/445.20 | 0.0159 | HOMO−2 → LUMO+1 (21%)<br>HOMO−1 → LUMO (21%)<br>HOMO−1 → LUMO+1 (32%)<br>HOMO → LUMO+2 (38%) | $B_{40}$ → $B_{40}$ and pyridine |
| Pyrazine-$B_{40}$ | $S_{12}$ | 3.00/413.41 | 0.0203 | HOMO−1 → LUMO+3 (53%) | $B_{40}$ → $B_{40}$ |
| | $S_9$ | 2.84/436.91 | 0.0957 | HOMO−4 → LUMO (27%)<br>HOMO−3 → LUMO (46%)<br>HOMO−1 → LUMO (22%) | $B_{40}$ → pyrazine |
| | $S_6$ | 2.72/455.26 | 0.0232 | HOMO−5 → LUMO (27%)<br>HOMO−2 → LUMO (42%) | $B_{40}$ → pyrazine |
| | $S_5$ | 2.70/459.75 | 0.0298 | HOMO−2 → LUMO (22%)<br>HOMO → LUMO+2 (55%) | $B_{40}$ → $B_{40}$ and pyrazine |
| Benzene-$B_{40}$-6 | $S_{29}$ | 3.65/339.9 | 0.0133 | HOMO−7 → LUMO+1 (51%)<br>HOMO−7 → LUMO+2 (27%) | $B_{40}$ → $B_{40}$ |
| | $S_{26}$ | 3.54/349.96 | 0.0834 | HOMO−6 → LUMO+1 (43%)<br>HOMO−5 → LUMO+2 (46%) | $B_{40}$ → $B_{40}$ |
| | $S_{10}$ | 3.09/401.75 | 0.0199 | HOMO → LUMO+3 (56%) | $B_{40}$ → $B_{40}$ |
| | $S_4$ | 2.87/431.86 | 0.0135 | HOMO−1 → LUMO (66%) | $B_{40}$ → $B_{40}$ |

other three typical absorption peaks are weaker, and localized around 413 nm, 455 nm and 460 nm, respectively. They are arising from the HOMO−5, HOMO−2, HOMO−1 and HOMO to LUMO, LUMO+2, and LUMO+3 transitions. The results indicate that the main adsorption peaks of pyrazine-$B_{40}$ originate from the $B_{40}$ to pyrazine transition. Compared with the absorption spectra of $B_{40}$ and pyridine-$B_{40}$ structures, the intensity of the absorption spectrum of pyrazine-$B_{40}$ is distinctly enhanced, and the absorption peak wavelength is redshifted to the visible light range. The redshift is caused by the main adsorption peak transition from HOMO−5 to LUMO+6. Compared to the $B_{40}$ (transition from HOMO−7 to LUMO+3), the transition MOs of pyrazine-$B_{40}$ transition to higher MO energy levels.

Moreover, the UV-vis absorption spectrum of $S_0 \rightarrow S_1$ for benzene-$B_{40}$-6 is shown in the green curve in Fig. 3a, and the data of four typical absorption peaks are also listed in Table 1. The first strong absorption peak is localized near 349.96 nm and originates from the HOMO−6 and HOMO−5 to LUMO+2 and LUMO+1 transition. The second strong absorption peak is localized near 401.75 nm and originates from the HOMO to LUMO+3 transitions. The other two typical absorption peaks are weaker, and locate around 339.90 nm and 431.86 nm, respectively. They originate from the HOMO−7 and HOMO−1 to LUMO, LUMO+1 and LUMO+2 transitions. The results show that the adsorption peaks of benzene-$B_{40}$-6 mainly transition from $B_{40}$ to $B_{40}$. Compared with the absorption spectra of pyridine-$B_{40}$ and pyrazine-$B_{40}$ structures, the intensity of the absorption spectrum of benzene-$B_{40}$-6 is weaker.

From the absorption spectra, it can be seen that pyridine adsorption can slightly redshift the main absorption peaks. The adsorbed pyrazine not only enhances the absorption spectrum of $B_{40}$, but also causes the absorption peaks of $B_{40}$ to redshift. However, the benzene adsorption has almost no effect on the absorption spectrum of $B_{40}$. This is because pyridine-$B_{40}$ and pyrazine-$B_{40}$ are chemisorption structures, the N atoms of pyridine and pyrazine are bonded to the B atoms of $B_{40}$. Further, the analysis of electron density difference indicates that there is electron accumulation at the bonding region and small molecules (pyridine and pyrazine), while there is electron dissipation on the $B_{40}$ that is close to the small molecules. However, the

Table 2 Fluorescence emission of $B_{40}$, pyridine-$B_{40}$, pyrazine-$B_{40}$, and benzene-$B_{40}$-6 structures

| Structures | States | $E/\lambda$ | $f$ | Main configuration (transitions) | Assignment |
|---|---|---|---|---|---|
| $B_{40}$ | $S_1$ | 2.48/500.05 | 0.0108 | LUMO → HOMO−1 (69%) | $B_{40}$ → $B_{40}$ |
| Pyridine-$B_{40}$ | $S_{10}$ | 2.72/456.03 | 0.0227 | LUMO → HOMO−5 (38%)<br>LUMO+1 → HOMO−3 (32%)<br>LUMO+1 → HOMO−1 (25%) | Pyridine → $B_{40}$; $B_{40}$ and pyridine → $B_{40}$ |
| | $S_9$ | 2.70/459.54 | 0.0281 | LUMO → HOMO−5 (27%)<br>LUMO+1 → HOMO−2 (24%)<br>LUMO+1 → HOMO−1 (41%) | Pyridine → $B_{40}$; $B_{40}$ and pyridine → $B_{40}$ |
| | $S_8$ | 2.60/477.39 | 0.0302 | LUMO → HOMO−5 (23%)<br>LUMO → HOMO−3 (39%)<br>LUMO → HOMO−2 (33%)<br>LUMO+3 → HOMO (33%) | Pyridine → $B_{40}$; $B_{40}$ and pyridine → $B_{40}$ |
| | $S_7$ | 2.54/488.17 | 0.0122 | LUMO+2 → HOMO (57%)<br>LUMO+3 → HOMO (22%) | $B_{40}$ → $B_{40}$; $B_{40}$ and pyridine → $B_{40}$ |
| Pyrazine-$B_{40}$ | $S_7$ | 2.49/497.74 | 0.0332 | LUMO+5 → HOMO (65%) | $B_{40}$ and pyrazine → $B_{40}$ |
| | $S_6$ | 2.37/522.32 | 0.0131 | LUMO → HOMO−2 (43%)<br>LUMO → HOMO−1 (51%) | Pyrazine → $B_{40}$ |
| | $S_4$ | 2.31/535.99 | 0.1132 | LUMO → HOMO−5 (29%)<br>LUMO → HOMO−2 (43%)<br>LUMO → HOMO−1 (42%) | Pyrazine → $B_{40}$ |
| Benzene-$B_{40}$-6 | $S_4$ | 2.65/467.73 | 0.0108 | LUMO → HOMO−1 (67%) | $B_{40}$ → $B_{40}$ |

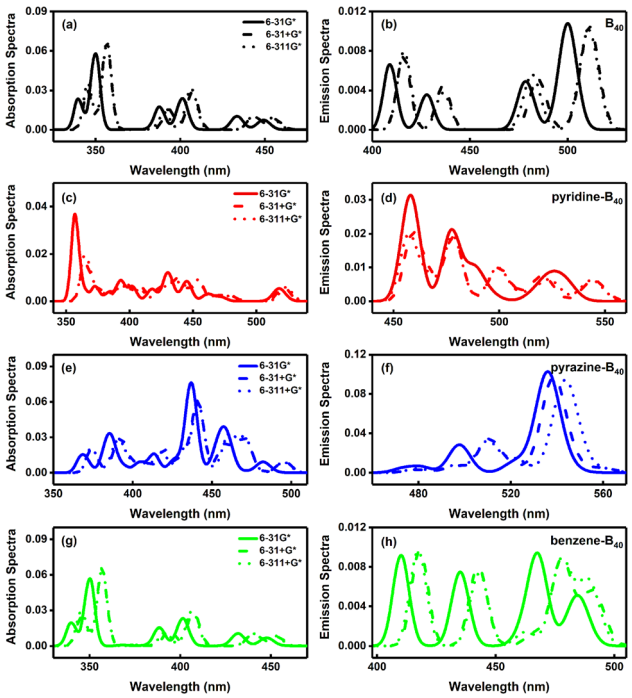


Fig. 4 The absorption and emission spectra of (a) and (b) $B_{40}$, (c) and (d) pyridine-$B_{40}$, (e) and (f) pyrazine-$B_{40}$ and (g) and (h) benzene-$B_{40}$-6 calculated by different basis sets. Solid, dash, and short dash lines represent the absorption and emission spectra calculated by CAM-B3LYP/6-31G*, CAM-B3LYP/6-31+G* and CAM-B3LYP/6-311+G*, respectively.

benzene-$B_{40}$-6 is physisorption structure, there is both electron accumulation and electron dissipation between benzene and $B_{40}$. The detailed diagram of electron density difference is shown in Fig. S1 in the ESI.† In other words, electrons are transferred from $B_{40}$ to small molecules for the pyridine-$B_{40}$ and pyrazine-$B_{40}$ structures, while for the benzene-$B_{40}$-6, there is no electron transfer between $B_{40}$ and benzene. This is consistent with the results of frontier MOs analysis.

To obtain the fluorescence emission properties of small molecule adsorbed on $B_{40}$, the single excited state of $B_{40}$, pyridine-$B_{40}$, pyrazine-$B_{40}$, and benzene-$B_{40}$-6 are also studied. The fluorescence emission spectra curves fitted by Gaussian function are shown in Fig. 3b. The lowest energy fluorescence emission wavelength of $B_{40}$ is around 500 nm (black curve), and the intensity of emission spectra of $B_{40}$ is weaker. For the pyridine-$B_{40}$ structure, the intensity of its emission spectrum is stronger than that of $B_{40}$. There are four typical emission spectra peaks of pyridine-$B_{40}$ around 456.03 nm, 459.54 nm, 477.39 nm and 488.17 nm, respectively, as see the red curve and dash lines in Fig. 3b. And the fluorescence emission peaks of pyridine-$B_{40}$ arises from the LUMO, LUMO+1, LUMO+2 and LUMO+3 to HOMO, HOMO−1, HOMO−2, HOMO−3 and HOMO−5 transition, which originates from the pyridine and $B_{40}$ to $B_{40}$ transition. The fluorescence emission wavelength and corresponding transition properties are listed in Table 2.

Furthermore, the lowest energy fluorescence emission of pyrazine-$B_{40}$ (blue curve in Fig. 3b) is significantly stronger than that of $B_{40}$ and the data of three typical emission peaks of pyrazine-$B_{40}$ is listed in Table 2. The first strong emission peak is near 536 nm and originates from LUMO to HOMO−1, HOMO−2 and HOMO−5 transition. The other two typical emission spectra peaks are near 497.74 nm and 522.32 nm, and they originate from the LUMO and LUMO+5 to HOMO, HOMO−1 and HOMO−2 transition. So the main emission peaks of pyrazine-$B_{40}$ originate from pyrazine to $B_{40}$ transition. For benzene-$B_{40}$-6 structure, the fluorescence emission is near 467.73 nm (green curve) and originates from the LUMO to HOMO−1 transition. And its fluorescence emission spectrum intensity is similar to that of $B_{40}$, but weaker than that of pyridine-$B_{40}$ and pyrazine-$B_{40}$. Thus, the absorption of pyridine and

pyrazine can enhance the emission spectrum of $B_{40}$, and they all in the visible light range. The fluorescence emission peaks of pyridine-$B_{40}$ and pyrazine-$B_{40}$ originate from small molecules to $B_{40}$ transition, while the fluorescence emission peak of benzene-$B_{40}$-6 originates from $B_{40}$ to $B_{40}$ transition.

Finally, we discussed the effect of the basis sets on the absorption and emission spectra. The absorption and emission spectra of $B_{40}$, pyridine-$B_{40}$, pyrazine-$B_{40}$, benzene-$B_{40}$-6 calculated by CAM-B3LYP/6-31G*, CAM-B3LYP/6-31+G* and CAM-B3LYP/6-311+G* are shown in Fig. 4. The results show that the intensity of absorption and emission spectra of $B_{40}$ calculated by 6-31+G* and 6-311+G* is stronger than that calculated by 6-31G*, and the main peaks of absorption and emission spectra calculated using 6-31+G* and 6-311+G* exhibit redshift relatively, as seen in Fig. 4a and b. And the absorption and emission spectra of $B_{40}$ calculated by 6-31+G* and 6-311+G* are almost identical. For pyridine-$B_{40}$, the intensity of absorption and emission spectra calculated by 6-31+G* and 6-311+G* is weaker than that calculated by 6-31G*, and the absorption peaks are also relative redshift (Fig. 4c and d). The absorption and emission spectra of pyrazine-$B_{40}$ calculated by 6-31G* are stronger than that calculated by 6-31+G* and 6-311+G* basis sets. And the main peaks of absorption and emission spectra calculated using 6-31+G* and 6-311+G* are redshift relatively, as shown in Fig. 4e and f. For benzene-$B_{40}$-6, the absorption and emission spectra calculated by 6-31+G* and 6-311+G* are stronger than that calculated by 6-31G*, and the main peaks occur to redshift (as seen in Fig. 4g and h). Thus, for different structures, the basis sets have different influence on the calculation of absorption and emission. But the main peaks of absorption and emission spectra calculated by the diffuse function augmented basis sets almost all undergo redshift. For the same structure, the influence of 6-31+G* and 6-311+G* basis sets on the calculation of absorption and emission spectra is almost same.

## Conclusions

This work, the adsorption and fluorescence emission spectra of pyridine-$B_{40}$, pyrazine-$B_{40}$ and benzene-$B_{40}$ are investigated by first principles. The results show that the adsorption of pyridine enhances the emission spectra of $B_{40}$. And the pyrazine adsorbed on $B_{40}$ not only enhance the adsorption and emission spectra of $B_{40}$, but also redshift the spectra to the visible light range. Moreover, the adsorbed benzene has almost no effect on the absorption and emission spectra of $B_{40}$. And the main adsorption peaks originate from the $B_{40}$ to small molecules and $B_{40}$ transition, and the main fluorescence emission peaks arise from small molecules to $B_{40}$ transition. However, benzene-$B_{40}$-6 is physisorption structure, its main adsorption and emission peaks originate from $B_{40}$ to $B_{40}$ transition. Finally, the influence on the calculation of 6-31G*, 6-31+G* and 6-311+G* basis sets on absorption and emission spectra are also studied, and the results indicate that the main peaks of absorption and emission spectra calculated by 6-31+G* and 6-311+G* basis sets occur to redshift.

It is well known that the emission spectra of quantum dots can cover the entire visible light region by changing the size and chemical composition of quantum dots.[30–33] The emission spectra of pyridine-$B_{40}$, pyrazine-$B_{40}$ and benzene-$B_{40}$-6 are in the visible range, so we believed that this work has potential applications in quantum dot luminescence, especially in the pyrazine-$B_{40}$ structure. To find inorganic and organic optical materials with good luminescent properties in the visible light range, many researchers focus on the electron absorption and emission of transition metal complexes.[34–36] While we studied luminescent materials from the perspective of the unique spectrum of superatoms. We hope this work provides a new perspective for luminescent materials.

## Author contributions

Jia Wang calculated and analyzed the results. All authors contributed to the general discussion.

## Conflicts of interest

There are no conflicts to declare.

## Acknowledgements

This work was financially supported by the Natural Science Foundation Project of Jilin Province (grant number YDZJ202101ZYTS075), the National Natural Science Foundation of China (grant number 11947039), the Education Department of Jilin Province (grant number JJKH20230510KJ).

## Notes and references

1 H.-J. Zhai, Y.-F. Zhao, W.-L. Li, Q. Chen, H. Bai, H.-S. Hu, Z. A. Piazza, W.-J. Tian, H.-G. Lu, Y.-B. Wu, Y.-W. Mu, G.-F. Wei, Z.-P. Liu, J. Li, S.-D. Li and L.-S. Wang, *Nat. Chem.*, 2014, **6**, 727–731.
2 J. Wang, T. Yu, Y. Gao and Z. Wang, *Sci. China Mater.*, 2017, **60**, 1264–1268.
3 J. Wang, W. Jiang, W. Xie, J. Wang and Z. Wang, *Sci. China Mater.*, 2019, **62**, 416–422.
4 N. Gonzalez Szwacki, A. Sadrzadeh and B. I. Yakobson, *Phys. Rev. Lett.*, 2007, **98**, 166804.
5 N. Gonzalez Szwacki, *Nanoscale Res. Lett.*, 2007, **3**, 49.
6 M. Keyhanian and D. Farmanzadeh, *J. Mol. Liq.*, 2019, **294**, 111638.
7 C. Tang and X. Zhang, *Int. J. Hydrogen Energy*, 2016, **41**, 16992–16999.
8 H. Dong, T. Hou, S. T. Lee and Y. Li, *Sci. Rep.*, 2015, **5**, 9952.
9 Y. Zhang, X. Han and X. Cheng, *Chem. Phys. Lett.*, 2020, **739**, 136961.
10 J. Mao, P. Guo, T. Zhang, S. Zhang and C. Liu, *Comput. Theor. Chem.*, 2020, **1181**, 112823.
11 M. Feng, J. Zhao and H. Petek, *Science*, 2008, **320**, 359–362.
12 W. D. Knight, K. Clemenger, W. A. De Heer, W. A. Saunders, M. Y. Chou and M. L. Cohen, *Phys. Rev. Lett.*, 1984, **53**, 510.
13 D. E. Bergeron, A. W. Castleman, T. Morisato and S. N. Khanna, *Science*, 2004, **304**, 84–87.

14 J. Li, X. Li, H. J. Zhai and L. S. Wang, *Science*, 2003, **299**, 864–867.
15 R. He and X. C. Zeng, *Chem. Commun.*, 2015, **51**, 3185–3188.
16 S.-X. Li, Z.-P. Zhang, Z.-W. Long and S.-J. Qin, *RSC Adv.*, 2017, **7**, 38526–38537.
17 E. Shakerzadeh, M. Yousefizadeh and M. Bamdad, *Inorg. Chem. Commun.*, 2020, **112**, 107692.
18 E. Shakerzadeh, Z. Biglari and E. Tahmasebi, *Chem. Phys. Lett.*, 2016, **654**, 76–80.
19 R. G. Parr, *Annu. Rev. Phys. Chem.*, 1983, **34**, 631–656.
20 Y. Yang, Z. Zhang, E. S. Penev and B. I. Yakobson, *Nanoscale*, 2017, **9**, 1805–1810.
21 S. Grimme, J. Antony, S. Ehrlich and H. Krieg, *J. Chem. Phys.*, 2010, **132**, 154104.
22 C. Adamo and V. Barone, *J. Chem. Phys.*, 1999, **110**, 6158–6170.
23 W. J. Hehre, R. Ditchfield and J. A. Pople, *J. Chem. Phys.*, 1972, **56**, 2257–2261.
24 M. A. Marques and E. K. Gross, *Annu. Rev. Phys. Chem.*, 2004, **55**, 427–455.
25 A. D. Laurent and D. Jacquemin, *Int. J. Quantum Chem.*, 2013, **113**, 2019–2039.
26 T. Yanai, D. P. Tew and N. C. Handy, *Chem. Phys. Lett.*, 2004, **393**, 51–57.
27 D. Kannar, A. Tajti and P. G. Szalay, *J. Chem. Theory Comput.*, 2017, **13**, 202–209.
28 M. J. Frisch, G. W. Trucks, H. B. Schlegel, G. E. Scuseria, M. A. Robb, J. R. Cheeseman, G. Scalmani, V. Barone, G. A. Petersson, H. Nakatsuji, X. Li, M. Caricato, A. V. Marenich, J. Bloino, B. G. Janesko, R. Gomperts, B. Mennucci, H. P. Hratchian, J. V. Ortiz, A. F. Izmaylov, J. L. Sonnenberg, F. D. Williams, F. Lipparini, F. Egidi, J. Goings, B. Peng, A. Petrone, T. Henderson, D. Ranasinghe, V. G. Zakrzewski, J. Gao, N. Rega, G. Zheng, W. Liang, M. Hada, M. Ehara, K. Toyota, R. Fukuda, J. Hasegawa, M. Ishida, T. Nakajima, Y. Honda, O. Kitao, H. Nakai, T. Vreven, K. Throssell, J. A. Montgomery Jr, J. E. Peralta, F. Ogliaro, M. J. Bearpark, J. J. Heyd, E. N. Brothers, K. N. Kudin, V. N. Staroverov, T. A. Keith, R. Kobayashi, J. Normand, K. Raghavachari, A. P. Rendell, J. C. Burant, S. S. Iyengar, J. Tomasi, M. Cossi, J. M. Millam, M. Klene, C. Adamo, R. Cammi, J. W. Ochterski, R. L. Martin, K. Morokuma, J. B. Foresman, O. Farkas and D. J. Fox, *Gaussian 16, Revision C.01*, Gaussian, Inc., Wallingford, CT, 2016.
29 Y. Gao, B. Wang, Y. Y. Lei, B. K. Teo and Z. G. Wang, *Nano Res.*, 2016, **9**, 622–632.
30 H. V. Han, H. Y. Lin, C. C. Lin, W. C. Chong, J. R. Li, K. J. Chen, P. Yu, T. M. Chen, H. M. Chen, K. M. Lau and H. C. Kuo, *Opt. Express*, 2015, **23**, 32504–32515.
31 J. Owen and L. Brus, *J. Am. Chem. Soc.*, 2017, **139**, 10939–10943.
32 L. Qian, Y. Zheng, J. Xue and P. H. Holloway, *Nat. Photonics*, 2011, **5**, 543–548.
33 Y. X. Yang, Y. Zheng, W. R. Cao, A. Titov, J. Hyvonen, J. R. Manders, J. G. Xue, P. H. Holloway and L. Qian, *Nat. Photonics*, 2015, **9**, 259–266.
34 T. Liu, B.-H. Xia, X. Zhou, Q.-C. Zheng, Q.-J. Pan and H.-X. Zhang, *Theor. Chem. Acc.*, 2008, **121**, 155–164.
35 K. J. Chen, H. V. Han, H. C. Chen, C. C. Lin, S. H. Chien, C. C. Huang, T. M. Chen, M. H. Shih and H. C. Kuo, *Nanoscale*, 2014, **6**, 5378–5383.
36 J. Shinar and R. Shinar, *J. Phys. D: Appl. Phys.*, 2008, **41**, 133001.